Magneto-optical trapping in a near-suface borehole

Vovrosh, Jamie; Wilkinson, Katie; Hedges, Sam; McGovern, Kieran; Hayati, Farzad; Carson, Christopher; Selyem, Adam; Winch, Jonathan; Stray, Ben; Earl, Luuk; Hamerow, Maxwell; Wilson, Georgia; Seedat, Adam; Roshanmanesh, Sanaz; Bongs, Kai; Holynski, Michael; Wu, Xuejian

DOI:
10.1371/journal.pone.0288353

Document Version
Publisher's PDF, also known as Version of record

Citation for published version (Harvard):
Vovrosh, J, Wilkinson, K, Hedges, S, McGovern, K, Hayati, F, Carson, C, Selyem, A, Winch, J, Stray, B, Earl, L, Hamerow, M, Wilson, G, Seedat, A, Roshanmanesh, S, Bongs, K, Holynski, M & Wu, X (ed.) 2023, 'Magneto-optical trapping in a near-suface borehole', *PLOS One*, vol. 18, no. 7, e0288353.
https://doi.org/10.1371/journal.pone.0288353

PLOS ONE

RESEARCH ARTICLE

Magneto-optical trapping in a near-suface borehole

Jamie Vovrosh[1], Katie Wilkinson[1], Sam Hedges[1], Kieran McGovern[1], Farzad Hayati[1], Christopher Carson[2], Adam Selyem[2], Jonathan Winch[1], Ben Stray[1], Luuk Earl[1], Maxwell Hamerow[1], Georgia Wilson[1], Adam Seedat[1], Sanaz Roshanmanesh[1], Kai Bongs[1], Michael Holynski[1]*

1 School of Physics and Astronomy, University of Birmingham, Birmingham, United Kingdom, **2** Fraunhofer Centre for Applied Photonics, Fraunhofer UK Research Ltd., Glasgow, United Kingdom

* m.holynski@bham.ac.uk

Citation: Vovrosh J, Wilkinson K, Hedges S, McGovern K, Hayati F, Carson C, et al. (2023) Magneto-optical trapping in a near-suface borehole. PLoS ONE 18(7): e0288353. https://doi.org/10.1371/journal.pone.0288353

Editor: Xuejian Wu, Rutgers University Newark, UNITED STATES

Received: January 31, 2023

Accepted: June 24, 2023

Published: July 11, 2023

Data Availability Statement: We have uploaded the minimal anonymized dataset necessary to replicate our study and findings to a stable, public repository. It can be accessed by following with the following DOI: 10.17605/OSF.IO/EG7HJ.

Funding: We acknowledge support from Engineering and Physical Sciences Research Council (EPSRC, https://www.ukri.org/councils/epsrc/) through grants EP/M013294/1 and EP/T001046/1 and Innovate UK (https://www.gov.uk/government/organisations/innovate-uk) through grants 133991 and 133989, as part of the UK

Abstract

Borehole gravity sensing can be used in a number of applications to measure features around a well, including rock-type change mapping and determination of reservoir porosity. Quantum technology gravity sensors, based on atom interferometry, have the ability to offer increased survey speeds and reduced need for calibration. While surface sensors have been demonstrated in real world environments, significant improvements in robustness and reductions to radial size, weight, and power consumption are required for such devices to be deployed in boreholes. To realise the first step towards the deployment of cold atom-based sensors down boreholes, we demonstrate a borehole-deployable magneto-optical trap, the core package of many cold atom-based systems. The enclosure containing the magneto-optical trap itself had an outer radius of (60 ± 0.1) mm at its widest point and a length of (890 ± 5) mm. This system was used to generate atom clouds at 1 m intervals in a 14 cm wide, 50 m deep borehole, to simulate how in-borehole gravity surveys are performed. During the survey, the system generated, on average, clouds of $(3.0 \pm 0.1) \times 10^5$ ^{87}Rb atoms with the standard deviation in atom number across the survey observed to be as low as 8.9×10^4.

Introduction

Gravity surveys are used to detect features through their density contrasts, and have an advantage over alternative techniques in that gravity is not attenuated by the intervening medium, such as borehole casing. In comparison with techniques such as ground penetrating radar or nuclear logging, this can allow for the detection of features at greater distances [1]. Additionally gravity sensing avoids the use of radioactive isotopes [2], mitigating security and health concerns. These benefits have led to gravity surveys being used in a number of environments to detect features of interest [3], including below the surface in boreholes. Borehole gravity sensing is used for a number of applications, including: remote sensing of gas and oil zones behind casing [4]; vertical density profiling for gravity map interpretation and for seismic modelling and analysis [5]; detection of geologic structures [6, 7]; determination of reservoir porosity for reserve estimates [8]; monitoring of reservoir fluid conditions for production

National Quantum Technologies Programme. The principle investigators of the grants used to fund this study where awarded to Kai Bongs and Michael Holynski. The funders had no role in study design, data collection and analysis, decision to publish, or preparation of the manuscript.

Competing interests: The authors have declared that no competing interests exist.

evaluation, and rock-type change mapping for groundwater and engineering studies [9, 10]; Carbon Capture and Storage (CCS) monitoring [11, 12]; as well as tests of fundamental physics [13, 14].

Despite numerous applications for borehole gravity sensing, a major drawback is measurement time when compared to other remote sensing techniques [15]. This is primarily due to the need to average out micro-seismic vibrations and calibrate for the inherent drift in existing sensors, via repeat measurements of the same point between sets of measurements. This limits its widespread use as a measurement technique. Quantum technology gravity and gravity gradient sensors based on atom interferometry [16, 17] have the potential to overcome these issues [18]. Moreover, gravity gradient sensors have the additional benefit of negating issues arising from micro-seismic noise [19].

Quantum technology based on atom interferometry has proven to be a powerful method for precision gravity sensing [17, 18, 20, 21], with sensitivities of 4.2 ng/$\sqrt{\text{Hz}}$ having been achieved in existing sensors [22]. Within laboratories, atom interferometry has enabled precise measurements of the equivalence principle [23], the fine-structure constant [24, 25], and the gravitational constant [26]. The demonstrated performance of laboratory systems and their inherent low drift has resulted in the development of a number of transportable atom interferometry systems targeting multiple applications and operational conditions [18, 19, 27–35].

Before atom-interferometry based-gravity sensors can be deployed down boreholes, a number of challenges need to be overcome. Borehole sensors have strict requirements on size, weight, and power consumption (SWaP), particularly for the radial size of the sensor. Existing borehole sensors typically have a radial diameter of between 10 mm—200 mm, usually set by the depth of operation. In addition to meeting the required SWaP, sensors need to be robust against environmental and operating conditions. Typically, the environmental conditions and operating requirements become more demanding the deeper the borehole. For example, in the deepest boreholes of up to 12 km [36], sensors can be required to operate at pressures of up to 1.4 kbar, temperatures of up to 200 ˚C and at angles from the vertical of up to 90˚. However for the majority of boreholes environmental conditions are much more hospitable, particularly in near surface boreholes.

In this article, for the first time, we demonstrate a compact magneto-optical trap (MOT). A MOT uses light that is detuned slightly below an atomic resonance in conjunction with a quadrupolar magnetic field, to cool and trap clouds of atoms [37]. The compact MOT system has the required SWaP and environmental robustness to be deployed in a borehole. This demonstrator was used to perform a simulated survey down a 14 cm diameter, 50 m deep, borehole where the water level was to within a few meters of the ground surface, to assess its robustness under trial conditions. During the deployment the system was able to, on average, produce clouds of $(3.0 \pm 0.1) \times 10^5$ ^{87}Rb atoms. MOTs form a core part of a number of cold atom-based devices including atomic clocks [38], accelerometers [39] and magnetometers [40]. As such, achieving a MOT meeting the form factor and robustness for in-borehole operation is the first step towards achieving a borehole-deployable cold atom-based sensor.

Borehole gravity surveys

Typically, borehole gravity measurements are collected at discrete intervals by stopping a deployed gravity sensor at predetermined observation depths and performing a stationary measurement [41], before moving to the next observation depth, as illustrated in Fig 1. From these measurements, the vertical gradient of gravity, $\Delta g/\Delta z$, is determined for the interval of interest by measuring the gravity difference, Δg, and the vertical distance between two consecutive stations, Δz. The subsurface layers are typically assumed to be infinitely extended

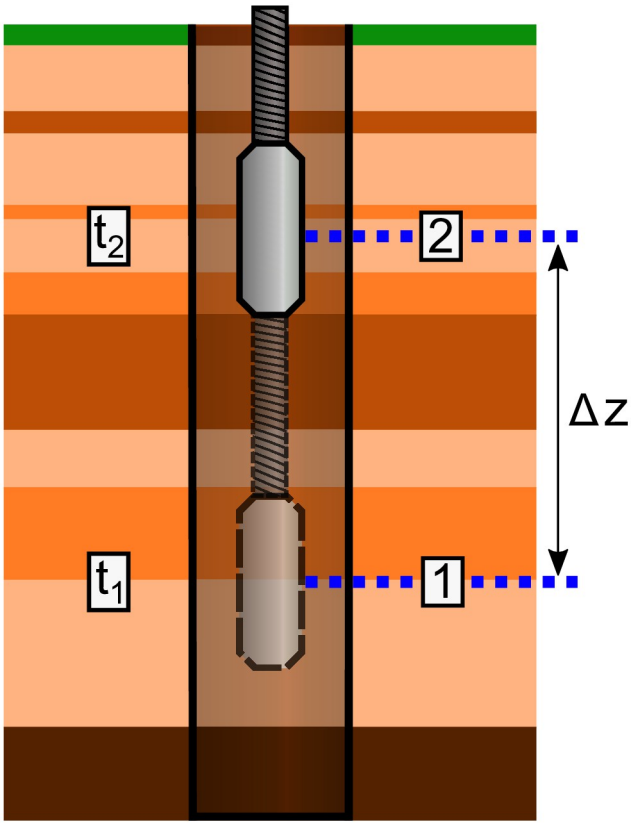

Fig 1. Schematic diagram of a borehole gravity sensing survey. In typical borehole gravity sensing, the sensor is lowered or raised to measurements points (denoted as 1 and 2) at fixed distances apart and measurements are performed when the sensor is stationary, with the data collected sequentially in time (t_i, where $i = 1, 2$).

https://doi.org/10.1371/journal.pone.0288353.g001

horizontal slabs of different densities, and the measurements between two points used to provide an average density of the region between each set of measurement points. For example, in Fig 1 the density measured between measurement points 1 and 2 would be the average of the various rock layers in-between.

Existing borehole gravity sensors used to perform such measurements typically rely on spring-based technology similar to that used in surface-based gravimeters [41]. To allow for operation down boreholes the technology used in surface-based sensors has been miniaturized, equipped with self-leveling capabilities and packaged to fit in narrow diameter borehole tools. For example, the sensor discussed in reference [41] has a radial diameter of 57 mm, can be used to depths of 2,500 m and its self leveling capabilities allow it to be deployed in boreholes inclined up to 30˚ from vertical. It is typically deployed by conducting wireline cable [41]. Atom interferometry based sensors will need to reach a similar or greater level of deployability to be a competitive tool across all of the applications in which gravity sensing is currently used.

To date, portable atom interferometry based gravity and gravity gradient sensors target surface-based applications and are consequently unsuitable for borehole deployment partly due to radial size and form factor. Several quantum technology-based gravity sensors comprise of a separate control system and sensor head [19, 29]. The control system typically contains the majority of electronics required to run the system, while the sensor head is the part of the system where the measurements take place. These two components are connected via an

umbilical, carrying optical and electronic signals. An early implementation could require that in-borehole atom interferometers have a control system on the surface. While this approach will work for shallow boreholes, it is expected that at certain length of the umbilical, systematics associated with having long optical fibres become a limitation (i.e optical power attenuation). As such, a control system capable of being deployed down a borehole will likely be required for operation at much greater depths. Initial implementations of quantum sensors are likely to operate in a similar manner to the existing borehole gravity sensors, stopping at intervals to perform measurements, with the long-term goal of performing measurements while moving [42], such that it can be used as a continuous logging tool. It is also expected that future quantum gravity sensors in borehole would be able to determine the gradient directly [43, 44], reducing errors associated with relative positioning between measurements [41].

As such, the demonstrator constructed here was designed to have the package deployed downhole while the control system remains on the surface. The science package was designed to be deployable via a winch, which was stopped at predefined intervals along the depth of the borehole to perform measurements. This allowed for an assessment of the variability and robustness of the system performance, while performing a simulated but representative survey.

Experimental system

The demonstrator consists of two sub-units (see Fig 2a), a control system and a science package, with optical and electrical signals transferred through a 75 m umbilical.

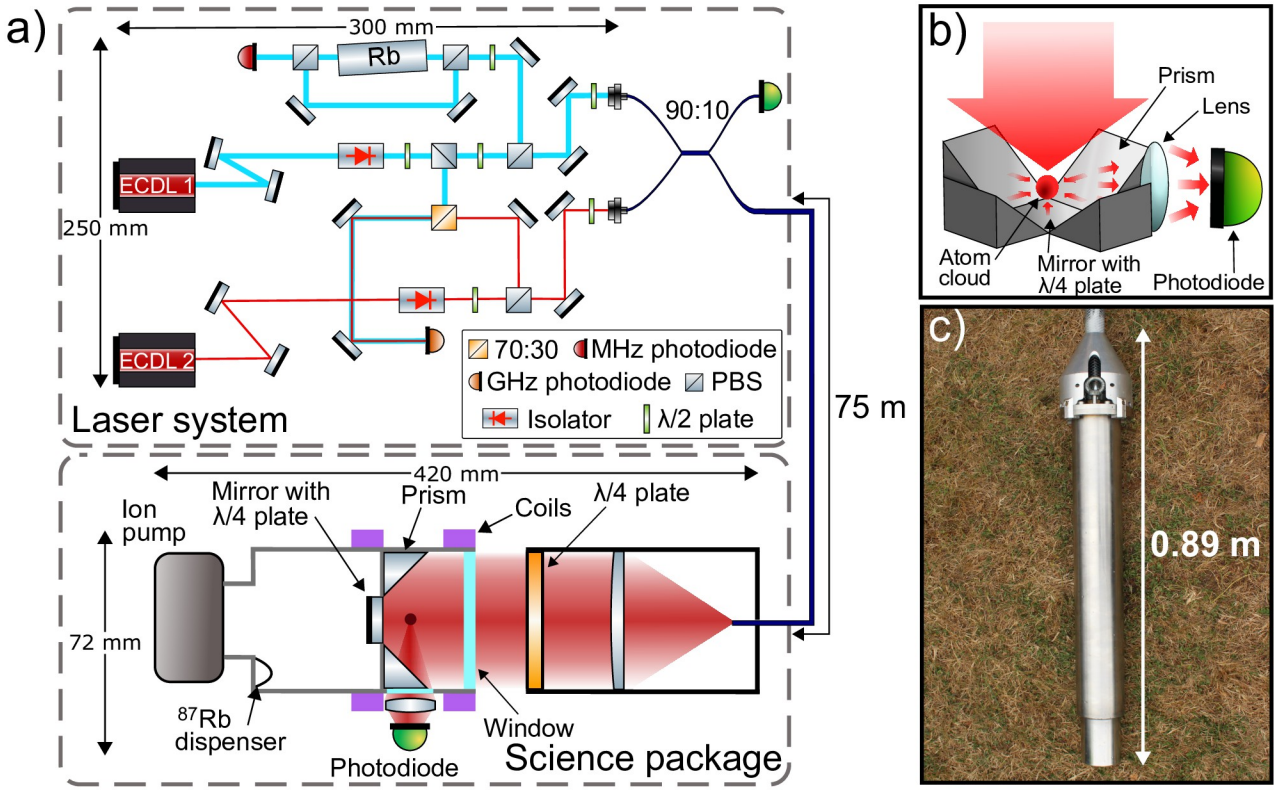

Fig 2. Laser system and science package diagram. a) Schematic diagram of the laser system and the science package (not to scale). b) Arrangement of the optics used to generate and measure the atom cloud (vacuum walls not shown). c) Photo of the science package. The vacuum system, optics and measurement photodiode are contained within the watertight stainless steel casing shown. The top of the science package is connected to the umbilical, which delivers the light and electrical signals required to operate the science package.

https://doi.org/10.1371/journal.pone.0288353.g002

The control system primarily consists of a laser system comprised of two Alter UK REMOTE external-cavity diode lasers (ECDLs) [45], each locked to different atomic transitions. ECDL 1 is used to produce repump light and is stabilised to a rubidium reference via saturated absorption spectroscopy [46, 47]. ECDL 2 is offset locked [48] to ECDL 1 and produces the light required for cooling. The repump is locked to the ^{87}Rb $|F = 1\rangle \rightarrow |F' = 2\rangle$ transition and the cooling laser is offset locked 6.5 GHz from the repump, approximately 10 MHz detuned below the $|F = 2\rangle \rightarrow |F' = 3\rangle$ transition.

Optical isolators are placed directly after the output of both ECDLs, providing 35 dB isolation to mitigate unwanted back reflections impacting the frequency performance of the ECDLs. The laser system has a pre-aligned saturated absorption spectroscopy setup where all the optics are bonded in place to provide a robust locking signal to stabilise the repump laser frequency. Separately, a small amount of light from both the cooling and repump beams are split off and overlapped on a fast photodiode to provide a beatnote for the offset lock. Various optics distribute laser light to two fibre couplers where the cooling and repump are combined using a 2x2, 90:10 fibre splitter. The laser system can produce a maximum power of 35 mW of cooling and 5 mW of repump light. During typical operation and in the survey, 12.8 mW cooling and 1.9 mW repump light was input into the umbilical fibre. The laser system is 250 mm x 300 mm x 80 mm in size, weighs 5 kg and uses robust mechanical mounting techniques to increase portability.

The light from this laser is delivered to the science package using a 75 m long polarisation-maintaining optical fibre. This fibre delivers the light to a telescope, which produces a circularly polarised beam with 16.6 mm $1/e^2$ diameter and an output power of approximately 8 mW, due to attenuation in the umbilical. This beam is collimated and shone directly into the vacuum chamber in which the four 5 mm × 5 mm prisms, a quarter wave plate, and a mirror are used to create the six counter-propagating beams required to cool the atoms in all three degrees of freedom (see Fig 2b) [49]. The use of a prism MOT reduces both the size of the optical delivery system and vacuum chamber, by reducing the number of optical inputs required, and the complexity of the laser system. Additionally, the use of a single input has the benefit that real and polarisation induced intensity noise are both common-mode between beam pairs. This enables highly stable atom cloud positions and temperatures overall, enhancing the system robustness. Coils are used to create a quadrupole magnetic field with a linear gradient and null field at the centre of the trapping region. The atoms are loaded into the trap from background atomic vapour, produced under vacuum with a rubidium dispenser. The scattered light from the atom cloud is measured through fluorescence detection. Vacuum pressure is maintained by a 0.4 ls^{-1} ion pump. The vacuum system, telescope and photo-diode have a form factor of (420 ± 1) mm × (72 ± 1) mm. To achieve this form factor techniques, such as indium sealing of vacuum windows, laser welding, and 3D printing of components were used alongside with custom electronics.

The science package is (420 ± 5) mm long and is contained in a (890 ± 5) mm long stainless steel waterproof enclosure (see Fig 2c), with an outer radius of (60 ± 0.1) mm at its widest point and internal radius of (37 ± 0.1) mm. The end of this enclosure consists of a solid stainless steel block to reduce buoyancy. This casing allows it to be deployed in cased or uncased boreholes and under waterlogged, muddy or dry borehole conditions. The science package is capable of surviving at temperatures of 60 ˚C, limited by the glass transition temperature of a few 3D printed polylactic acid parts. Replacing these with aluminium would enable operation at higher temperatures. The science package is expected to be waterproof to pressures of ≈100 bar. The science package does not require centralisation.

Deployment campaign

The system was transported in a medium-sized van, a short distance from the lab to the University of Birmingham campus borehole test site [50, 51] for deployment down a borehole as shown in Fig 3a. During transport the system was unpowered. The optical system was found to be robust, remaining aligned throughout transport without the need for realignment at the survey site. The borehole itself is 50 m deep and cased to a depth of 12 m with an internal diameter of 14 cm in the cased section (see Fig 3b). The groundwater level was (3.59 ± 0.02) m below the ground surface level at the time of the survey, determined via the use of a water level meter. No permits were required to carry out the survey as the borehole site is located on the university's campus.

Once at the site, the science package was attached to a cable via the eye holes on the top of the package and lowered into the borehole using a winch and tripod (see Fig 3c). At intervals of (1 ± 0.02) m below the surface the system was stopped and 5 MOT loading curves were taken. On average, 2 minutes were spent at each depth to record data, limited by the data capture of the oscilloscope used. Moving the system between depths took approximately 4 minutes, limited by the speed of the winch used.

During the survey the stability of the number of atoms in the MOT was measured for 400 s on the surface as well as at the middle, (25.34 ± 0.02) m and bottom, (49.34 ± 0.02) m of the borehole. The variation in atom number (ΔN) relative to the start each of time period is shown in Fig 4. The standard deviations at the surface, middle and bottom positions (shown in Fig 4) were 1.1×10^5, 1.1×10^5 and 1.1×10^5 respectively, suggesting that the MOT stability on short time scales in the borehole and on the surface were comparable. The atom number over the

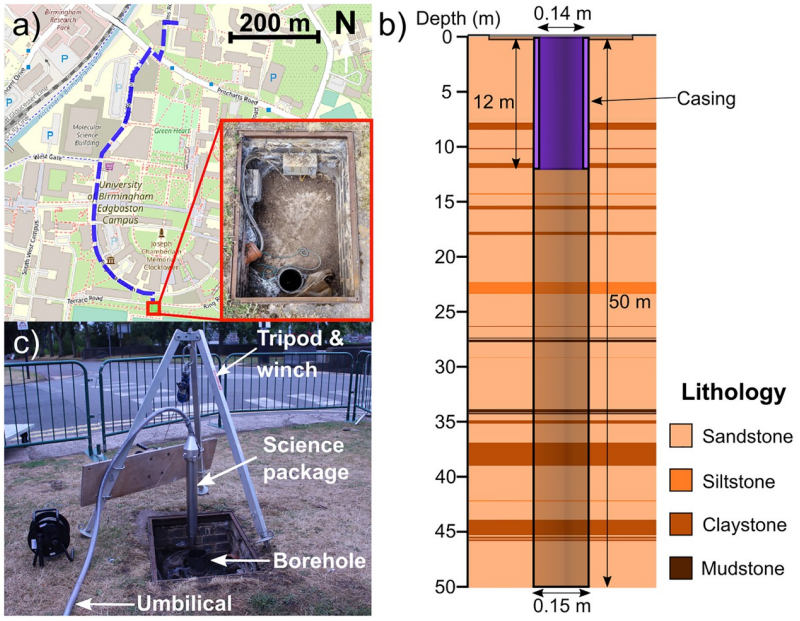

Fig 3. Borehole where the survey was conducted. a) The location of the test site and route driven to the test site (shown by the blue dashed line). Map data from © OpenStreetMap under the Open Database Licence [53]. The surface of the borehole used for the deployment campaign, is shown in the inset photo (red border). b) Diagram showing the dimensions and lithology of the borehole used in the deployment campaign. The lithological data was obtained from geophysical logging (natural gamma and electrical resistivity), combined with core examination. c) The winch and tripod system used to lower the science package into the borehole. A wire with markings at 1 m intervals was used to record the depth of the device.

https://doi.org/10.1371/journal.pone.0288353.g003

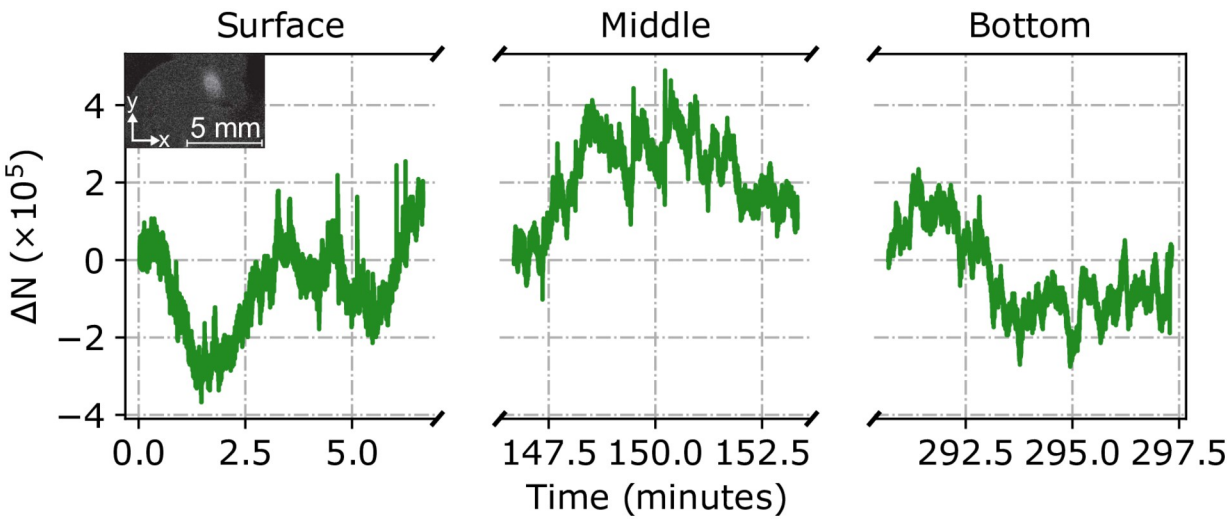

Fig 4. Variation of the atom number at different depths. The atom number variation with time, relative to the first measurement in each time period, on the surface and at depths of (25.34 ± 0.02) m and (49.34 ± 0.02) m in the borehole. The inset photo shows a photo of the cloud on the surface with a radius ($1/e^2$) of (0.81 ± 0.08) mm in the x-direction and (1.1 ± 0.1) mm in the y-direction.

https://doi.org/10.1371/journal.pone.0288353.g004

whole deployment had a standard deviation of 8.9×10^4, suggesting that the variation in atom number on short and long time scales was similar.

The atom number and loading time constant averaged over 5 curves at each depth can be seen in Fig 5. The loading time constant over the course of the deployment had a standard deviation of 5.00 ms, demonstrating a good level of repeatability. The average atom number achieved in the system over the course of the deployment was $(3.0 \pm 0.1) \times 10^5$, with an average loading time constant of (24.8 ± 0.2) ms. After reaching a depth of (49.34 ± 0.02) m and completing all data acquisition, the system was brought back to the surface. The MOT was maintained throughout the trial and was robust to all of the moving and stopping, with no statistically significant effect on the atom cloud observed when becoming submerged under water or exiting the cased part of the borehole. The variation in atom number and loading time can be attributed to variation in polarisation and the intensity of the light used to create the MOT. This variation is caused by temperature and stress on the 75 m optical fibre used to deliver light into the science package. This could be addressed in future systems with polarisation stabilisation and correction systems [52].

During the trial the pressure in the vacuum chamber varied between 6.5×10^{-7} mbar and 7.7×10^{-7} mbar estimated from the ion pump. This level of variation is typical of performance seen during operation in the lab. The average background pressure over the course of the survey in the MOT region is estimated from the MOT to be $1.1 \pm 0.3 \times 10^{-6}$ mbar using method in reference [54]. While these pressures allow for the generation of a MOT, future systems will need to improve the pressure in the system for any practical uses.

Conclusions and outlook

The high-precision and low-drift measurements offered by atom interferometry-based gravity sensors, once realised in borehole-deployable packages, have the potential to open up new sensing capabilities, particularly for long-term monitoring applications such as CCS [56] and hydrological monitoring. To push cold atom-based sensors towards the SWaP profile and

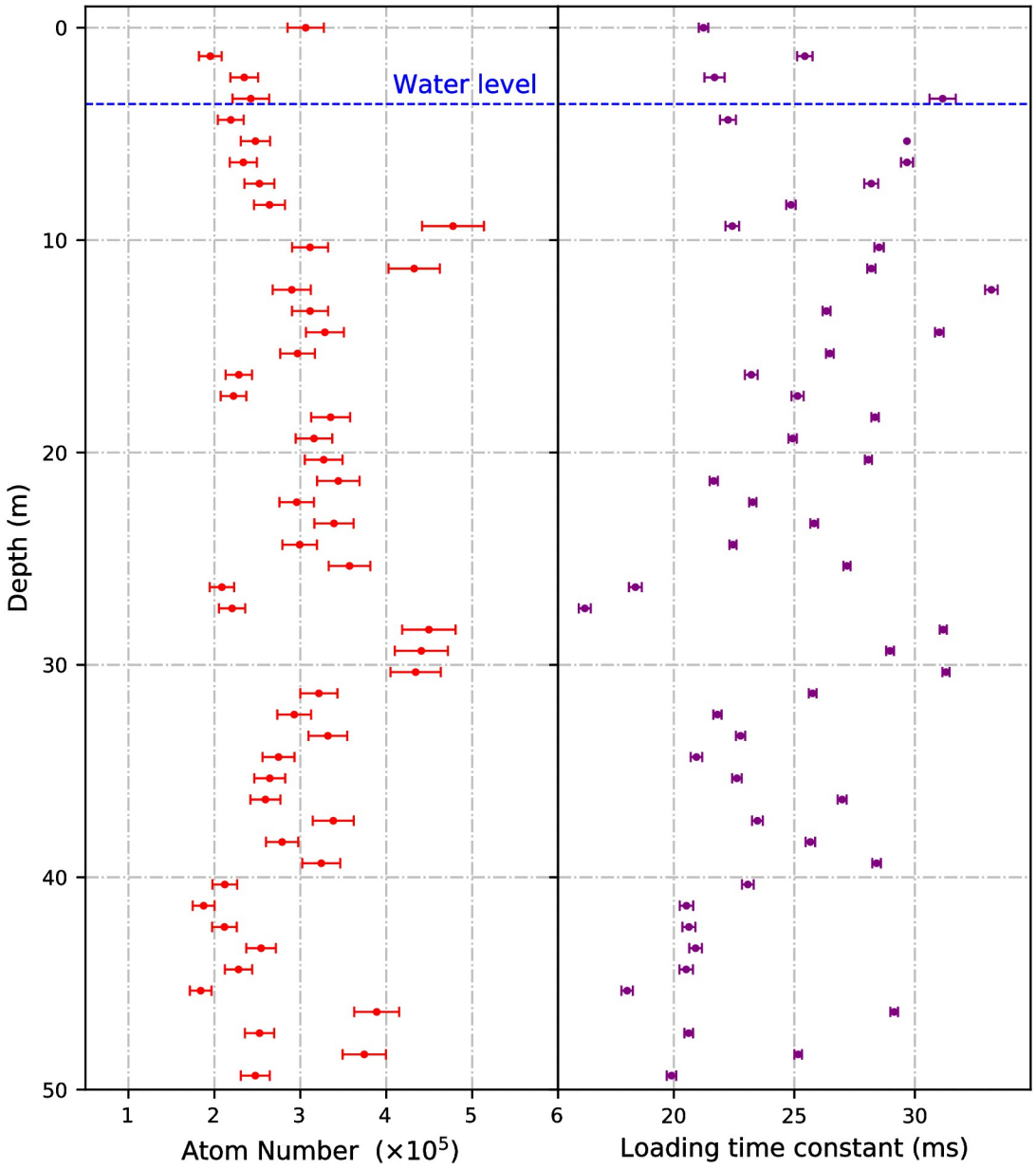

Fig 5. MOT parameters as a function of depth in the borehole. The atom numbers and loading time constants were determined by fitting equation 2 from reference [55] to loading curves taken at each depth, with the leading source of error attributed to the voltage to atom number conversion. The depths were measured with an error of ±0.02 m.

https://doi.org/10.1371/journal.pone.0288353.g005

robustness that is required for deployment and operation in boreholes, the first borehole-deployable cold atom system has been developed and trialed.

The system was demonstrated to be capable of generating clouds of laser-cooled ^{87}Rb atoms in a system package of (890 ± 5) mm × (120 ± 1) mm diameter. The system successfully operated down a 50 m deep borehole, generating atom clouds with an average of (3.0 ± 0.1) × 10^5 atoms. The standard deviation in atom number performance across the survey was 8.9 × 10^4 atoms. The performance in terms of number of atoms in the trap and atom number stability

were comparable to the device performance on the surface and comparable to MOTs used in some existing cold atom sensors [27, 31, 40].

To upgrade the demonstrator shown here to a full sensor capable of gravity measurements, several extensions to the system (i.e additional functionality in the laser, magnetic shielding). For example, to implement a sub-Doppler cooling stage in the system, In addition of adding functionality to the laser, upgrades to the science package to include shielding and/or cancellation fields would be required. Upgrades such as these would need to meet the requirements for operation down a borehole. These requirements include meeting sufficiently small SWaP and robustness for deployment (e.g. operation while tilted from the vertical), both of which are active research areas. Examples of innovations which could be utilised to produce SWaP optimised sensors for borehole deployment include SWaP optimised 3D printed components [57–59] and passively pumped vacuum cells [54, 60, 61] to allow for operation in shallow boreholes. Further miniaturisation is required to remove the need for a surface based control system and allow for deployment in deeper boreholes, i.e. compact laser systems [62–64].

It is also possible that significant improvements in performance over current state of the art laboratory and portable systems may be possible, through the incorporation of the latest and future techniques [65–69] and technological developments [49, 70–72].

Acknowledgments

We would like to acknowledge significant support from John Tellam in regards to planning and carrying out the trial. We would also like to acknowledge Alter UK for providing the packaged ECDLs, as well as technical support from the University of Birmingham Engineering and Physical Sciences workshop. Map data copyrighted OpenStreetMap contributors and available from https://www.openstreetmap.org.

Author Contributions

Conceptualization: Jamie Vovrosh.

Data curation: Jamie Vovrosh, Katie Wilkinson, Adam Selyem.

Formal analysis: Jamie Vovrosh, Katie Wilkinson.

Funding acquisition: Jamie Vovrosh, Christopher Carson, Kai Bongs, Michael Holynski.

Investigation: Jamie Vovrosh, Katie Wilkinson, Sam Hedges, Kieran McGovern, Farzad Hayati, Christopher Carson, Adam Selyem, Jonathan Winch, Ben Stray, Luuk Earl, Maxwell Hamerow, Georgia Wilson, Adam Seedat, Sanaz Roshanmanesh.

Methodology: Jamie Vovrosh.

Project administration: Jamie Vovrosh.

Resources: Jamie Vovrosh.

Software: Jamie Vovrosh, Katie Wilkinson.

Supervision: Jamie Vovrosh, Kai Bongs, Michael Holynski.

Validation: Jamie Vovrosh, Katie Wilkinson, Sam Hedges, Jonathan Winch, Ben Stray.

Visualization: Jamie Vovrosh, Katie Wilkinson.

Writing – original draft: Jamie Vovrosh.

Writing – review & editing: Jamie Vovrosh, Katie Wilkinson, Sam Hedges, Kieran McGovern, Farzad Hayati, Christopher Carson, Adam Selyem, Jonathan Winch, Ben Stray, Luuk

Earl, Maxwell Hamerow, Georgia Wilson, Adam Seedat, Sanaz Roshanmanesh, Kai Bongs, Michael Holynski.

References

1. Boddice D, Metje N, Tuckwell G. Capability assessment and challenges for quantum technology gravity sensors for near surface terrestrial geophysical surveying. Journal of Applied Geophysics. 2017; 146:149–159. https://doi.org/10.1016/j.jappgeo.2017.09.018
2. Mills WR, Stromswold DC, Allen LS. Advances in nuclear oil well logging. Nuclear Geophysics. 1991; 5 (3):209–227.
3. Fairhead JD, Odegard ME. Advances in gravity survey resolution. The Leading Edge. 2002; 21(1):36–37. https://doi.org/10.1190/1.1445845
4. Cho Y, Cao Y, Zagayevskiy Y, Wong T, Munoz Y. Kriging-based monitoring of reservoir gas saturation distribution using time-lapse multicomponent borehole gravity measurements: Case study, Hastings Field. Journal of Petroleum Science and Engineering. 2020; 190:107054. https://doi.org/10.1016/j.petrol.2020.107054
5. Lines LR, Tan H, Schultz AK. Cross-borehole analysis of velocity and density. Geoexploration. 1991; 28(3):183–191. https://doi.org/10.1016/0016-7142(91)90033-9
6. Beyer LA, Clutsom FG. Borehole gravity survey in the Dry Piney oil and gas field, Big Piney-La Barge area, Sublette County, Wyoming. US Geol Surv, Oil Gas Invest, Chart; (United States). 1978;.
7. Nekut AG. Borehole gravity gradiometry. GEOPHYSICS. 1989; 54(2):225–234. https://doi.org/10.1190/1.1442646
8. Beyer LA, Clutsom F. Density and porosity of oil reservoirs and overlying formations from borehole gravity measurements, Gebo Oil Field, Hot Springs County, Wyoming. 1978;.
9. Halley RB, Schmoker JW. High-Porosity Cenozoic Carbonate Rocks of South Florida: Progressive Loss of Porosity with Depth. AAPG Bulletin. 1983; 67(2):191–200. https://doi.org/10.1306/03B5ACE6-16D1-11D7-8645000102C1865D
10. LaFehr T. Rock density from borehole gravity surveys. Geophysics. 1983; 48(3):341–356. https://doi.org/10.1190/1.1441472
11. Appriou D, Bonneville A, Zhou Q, Gasperikova E. Time-lapse gravity monitoring of CO2 migration based on numerical modeling of a faulted storage complex. International Journal of Greenhouse Gas Control. 2020; 95:102956. https://doi.org/10.1016/j.ijggc.2020.102956
12. Dodds K, Krahenbuhl R, Reitz A, Li Y, Hovorka S. Evaluating time-lapse borehole gravity for CO2 plume detection at SECARB Cranfield. International Journal of Greenhouse Gas Control. 2013; 18:421–429. https://doi.org/10.1016/j.ijggc.2013.05.024
13. Thomas J, Vogel P. Testing the inverse-square law of gravity in boreholes at the Nevada Test Site. Phys Rev Lett. 1990; 65:1173–1176. https://doi.org/10.1103/PhysRevLett.65.1173 PMID: 10042193
14. Ander ME, Zumberge MA, Lautzenhiser T, Parker RL, Aiken CLV, Gorman MR, et al. Test of Newton's inverse-square law in the Greenland ice cap. Phys Rev Lett. 1989; 62:985–988. https://doi.org/10.1103/PhysRevLett.62.985 PMID: 10040395
15. Hinton A, Perea-Ortiz M, Winch J, Briggs J, Freer S, Moustoukas D, et al. A portable magneto-optical trap with prospects for atom interferometry in civil engineering. Philosophical Transactions of the Royal Society A: Mathematical, Physical and Engineering Sciences. 2017; 375(2099):20160238. https://doi.org/10.1098/rsta.2016.0238 PMID: 28652493
16. Kasevich M, Chu S. Atomic interferometry using stimulated Raman transitions. Phys Rev Lett. 1991; 67:181–184. https://doi.org/10.1103/PhysRevLett.67.181 PMID: 10044515
17. Peters Achim, Chung Yeow K, Chu Steven. Measurement of gravitational acceleration by dropping atoms. Nature. 1999; 400:849–. https://doi.org/10.1038/23655
18. Bongs K, Holynski M, Vovrosh J, Bouyer P, Condon G, Rasel E, et al. Taking atom interferometric quantum sensors from the laboratory to real-world applications. Nat Rev Phys. 2019; 1(12):731–739. https://doi.org/10.1038/s42254-019-0117-4
19. Stray B, Lamb A, Kaushik A, Vovrosh J, Rodgers A, Winch J, et al. Quantum sensing for gravitational cartography. Nature. 2022; 602:590–594. https://doi.org/10.1038/s41586-021-04315-3 PMID: 35197616
20. Dickerson SM, Hogan JM, Sugarbaker A, Johnson DMS, Kasevich MA. Multiaxis Inertial Sensing with Long-Time Point Source Atom Interferometry. Phys Rev Lett. 2013; 111:083001. https://doi.org/10.1103/PhysRevLett.111.083001 PMID: 24010433

21. Peters A, Chung KY, Chu S. High-precision gravity measurements using atom interferometry. Metrologia. 2001; 38(1):25–61. https://doi.org/10.1088/0026-1394/38/1/4

22. Hu ZK, Sun BL, Duan XC, Zhou MK, Chen LL, Zhan S, et al. Demonstration of an ultrahigh-sensitivity atom-interferometry absolute gravimeter. Phys Rev A. 2013; 88:043610. https://doi.org/10.1103/PhysRevA.88.043610

23. Asenbaum P, Overstreet C, Kim M, Curti J, Kasevich MA. Atom-Interferometric Test of the Equivalence Principle at the 10^{-12} Level. Phys Rev Lett. 2020; 125:191101. https://doi.org/10.1103/PhysRevLett.125.191101 PMID: 33216577

24. Morel L, Yao Z, Cladé P, Guellati-Khélifa S. Determination of the fine-structure constant with an accuracy of 81 parts per trillion. Nature. 2020; 588(7836):61–65. https://doi.org/10.1038/s41586-020-2964-7 PMID: 33268866

25. Parker RH, Yu C, Zhong W, Estey B, Müller H. Measurement of the fine-structure constant as a test of the Standard Model. Science (New York, NY). 2018; 360(6385):191–195. https://doi.org/10.1126/science.aap7706 PMID: 29650669

26. Rosi G, Sorrentino F, Cacciapuoti L, Prevedelli M, Tino GM. Precision measurement of the Newtonian gravitational constant using cold atoms. Nature. 2014; 510:518–521. https://doi.org/10.1038/nature13433 PMID: 24965653

27. Bidel Y, Zahzam N, Blanchard C, Bonnin A, Cadoret M, Bresson A, et al. Absolute marine gravimetry with matter-wave interferometry. Nature Communications. 2018; 9. https://doi.org/10.1038/s41467-018-03040-2 PMID: 29434193

28. Becker D, Lachmann MD, Seidel ST, Ahlers H, Dinkelaker AN, Grosse J, et al. Space-borne Bose–Einstein condensation for precision interferometry. Nature. 2018; 562. https://doi.org/10.1038/s41586-018-0605-1 PMID: 30333576

29. Menoret V, Vermeulen P, Moigne NL, Bonvalot S, Bouyer P, Landragin A, et al. Gravity measurements below 10^{-9} *g* with a transportable absolute quantum gravimeter. Sci Rep. 2018; 8(12300). https://doi.org/10.1038/s41598-018-30608-1

30. Wu X, Pagel Z, Malek BS, Nguyen TH, Zi F, Scheirer DS, et al. Gravity surveys using a mobile atom interferometer. Science Advances. 2019; 5(9). https://doi.org/10.1126/sciadv.aax0800 PMID: 31523711

31. Bidel Y, Zahzam N, Bresson A, Blanchard C, Cadoret M, Olesen AV, et al. Absolute airborne gravimetry with a cold atom sensor. Journal of Geodesy. 2020; 94. https://doi.org/10.1007/s00190-020-01350-2

32. Guo J, Ma S, Zhou C, Liu J, Wang B, Pan D, et al. Vibration Compensation for a Vehicle-mounted Atom Gravimeter. 2021. https://doi.org/10.20944/preprints202111.0255.v1

33. Earl L, Vovrosh J, Wright M, Roberts D, Winch J, Perea-Ortiz M, et al. Demonstration of a Compact Magneto-Optical Trap on an Unstaffed Aerial Vehicle. Atoms. 2022; 10(1). https://doi.org/10.3390/atoms10010032

34. Wang H, Wang K, Xu Y, Tang Y, Wu B, Cheng B, et al. A Truck-Borne System Based on Cold Atom Gravimeter for Measuring the Absolute Gravity in the Field. Sensors. 2022; 22(16). https://doi.org/10.3390/s22166172 PMID: 36015933

35. Templier S, Cheiney P, d'Armagnac de Castanet Q, Gouraud B, Porte H, Napolitano F, et al. Tracking the vector acceleration with a hybrid quantum accelerometer triad. Science Advances. 2022; 8(45): eadd3854. https://doi.org/10.1126/sciadv.add3854 PMID: 36351013

36. Kozlovsky YA, Adrianov N. The superdeep well of the Kola Peninsula. Springer; 1987.

37. Steane AM, Chowdhury M, Foot CJ. Radiation force in the magneto-optical trap. J Opt Soc Am B. 1992; 9(12):2142–2158. https://doi.org/10.1364/JOSAB.9.002142

38. Diddams SA, Udem T, Bergquist J, Curtis E, Drullinger R, Hollberg L, et al. An optical clock based on a single trapped 199Hg+ ion. Science. 2001; 293(5531):825–828. https://doi.org/10.1126/science.1061171 PMID: 11452082

39. Narducci FA, Black AT, Burke JH. Advances toward fieldable atom interferometers. Advances in Physics: X. 2022; 7(1):1946426. https://doi.org/10.1080/23746149.2021.1946426

40. Behbood N, Martin Ciurana F, Colangelo G, Napolitano M, Mitchell MW, Sewell RJ. Real-time vector field tracking with a cold-atom magnetometer. Applied Physics Letters. 2013; 102(17):173504. https://doi.org/10.1063/1.4803684

41. Nind C, MacQueen J, Wasylechko R, Chemam M, Nackers C. GRAVILOG -An update on the development and use of Borehole Gravity for Mining Exploration. 2013; p. 1–5. https://doi.org/10.1071/ASEG2013ab048

42. Adams B, Macrae C, Entezami M, Ridley K, Kubba A, Lien YH, et al. The development of a High data rate atom interferometric gravimeter (HIDRAG) for gravity map matching navigation. In: 2021 IEEE International Symposium on Inertial Sensors and Systems (INERTIAL); 2021. p. 1–4.

43. Snadden MJ, McGuirk JM, Bouyer P, Haritos KG, Kasevich MA. Measurement of the Earth's Gravity Gradient with an Atom Interferometer-Based Gravity Gradiometer. Phys Rev Lett. 1998; 81:971–974. https://doi.org/10.1103/PhysRevLett.81.971

44. McGuirk JM, Foster GT, Fixler JB, Snadden MJ, Kasevich MA. Sensitive absolute-gravity gradiometry using atom interferometry. Phys Rev A. 2002; 65:033608. https://doi.org/10.1103/PhysRevA.65.033608

45. Dorward W, Lee ST, Bremner D, Robertson S, Jones B, Carson C, et al. The application of telecoms-style packaging techniques to narrow linewidth laser modules for quantum technologies. In: Components and Packaging for Laser Systems V. vol. 10899 of Society of Photo-Optical Instrumentation Engineers (SPIE) Conference Series; 2019. p. 1089908.

46. Lee KI, Kim JA, Noh HR, Jhe W. Single-beam atom trap in a pyramidal and conical hollow mirror. Opt Lett. 1996; 21(15):1177–1179. https://doi.org/10.1364/OL.21.001177 PMID: 19876291

47. MacAdam KB, Steinbach A, Wieman C. A narrow-band tunable diode laser system with grating feedback, and a saturated absorption spectrometer for Cs and Rb. American Journal of Physics. 1992; 60 (12):1098–1111. https://doi.org/10.1119/1.16955

48. Schünemann U, Engler H, Grimm R, Weidemüller M, Zielonkowski M. Simple scheme for tunable frequency offset locking of two lasers. Review of Scientific Instruments. 1999; 70(1):242–243. https://doi.org/10.1063/1.1149573

49. Vovrosh J, Earl L, Thomas H, Winch J, Stray B, Ridley K, et al. Reduction of background scattered light in vacuum systems for cold atoms experiments. AIP Advances. 2020; 10(10):105125. https://doi.org/10.1063/5.0030041

50. Bouch JE, Hough E, Kemp SJ, McKervey JA, Williams GM, Gresswell RB. Sedimentary and diagenetic environments of the Wildmoor Sandstone Formation (UK): implications for groundwater and contaminant transport, and sand production. In: Barker RD, Tellam JH, editors. Fluid flow and solute movements in sandstones: the onshore UK Permo-Triassic red bed sequence. vol. 263 of Geological Society Special Publications. London, UK: Geological Society of London; 2006. p. 129–153. Available from: http://nora.nerc.ac.uk/id/eprint/19549/.

51. Riley MS, Tellam JH, Greswell RB, Durand V, Aller MF. Convergent tracer tests in multilayered aquifers: The importance of vertical flow in the injection borehole. Water Resources Research. 2011; 47(7). https://doi.org/10.1029/2010WR009838

52. Niggebaum A. Towards mobile quantum sensors for gravity surveys. University of Birmingham; 2016.

53. OpenStreetMap contributors. OpenStreetMap. Available under the Open DatabaseLicence from: https://www.openstreetmap.org.

54. Little BJ, Hoth GW, Christensen J, Walker C, De Smet DJ, Biedermann GW, et al. A passively pumped vacuum package sustaining cold atoms for more than 200 days. AVS Quantum Science. 2021; 3 (3):035001. https://doi.org/10.1116/5.0053885

55. Moore RWG, Lee LA, Findlay EA, Torralbo-Campo L, Bruce GD, Cassettari D. Measurement of vacuum pressure with a magneto-optical trap: A pressure-rise method. Review of Scientific Instruments. 2015; 86(9):093108. https://doi.org/10.1063/1.4928154 PMID: 26429430

56. Ridley K, de Villiers G, Vovrosh J, Vincent C, Wilkinson P, Holynski M. Quantum Technology Based Gravity and Gravity Gradiometry as a Tool for CCS Monitoring and Investigation. Proceedings of the 16th Greenhouse Gas Control Technologies Conference (GHGT-16). 2022;48(3):341–356.

57. Vovrosh J, Voulazeris G, Petrov PG, Zou J, Gaber Y, Benn L, et al. Additive manufacturing of magnetic shielding and ultra-high vacuum flange for cold atom sensors. Sci Rep. 2018; 8. https://doi.org/10.1038/s41598-018-20352-x PMID: 29386536

58. Cooper N, Coles LA, Everton S, Maskery I, Campion RP, Madkhaly S, et al. Additively manufactured ultra-high vacuum chamber for portable quantum technologies. Addit Manuf. 2021; 40:101898. https://doi.org/10.1016/j.addma.2021.101898

59. Madkhaly SH, Coles LA, Morley C, Colquhoun CD, Fromhold TM, Cooper N, et al. Performance-Optimized Components for Quantum Technologies via Additive Manufacturing. PRX Quantum. 2021; 2:030326. https://doi.org/10.1103/PRXQuantum.2.030326

60. Rushton J, Aldous M, Himsworth M. Contributed review: The feasibility of a fully miniaturized magneto-optical trap for portable ultracold quantum technology. Review of Scientific Instruments. 2014; 85 (12):121501. https://doi.org/10.1063/1.4904066 PMID: 25554265

61. Burrow OS, Osborn PF, Boughton E, Mirando F, Burt DP, Griffin PF, et al. Stand-alone vacuum cell for compact ultracold quantum technologies. Applied Physics Letters. 2021; 119(12):124002. https://doi.org/10.1063/5.0061010

62. Theron F, Bidel Y, Dieu E, Zahzam N, Cadoret M, Bresson A. Frequency-doubled telecom fiber laser for a cold atom interferometer using optical lattices. Optics Communications. 2017; 393:152–155. https://doi.org/10.1016/j.optcom.2017.02.013

63. Luo Q, Zhang H, Zhang K, Duan XC, Hu ZK, Chen LL, et al. A compact laser system for a portable atom interferometry gravimeter. Review of Scientific Instruments. 2019; 90(4):043104. https://doi.org/10.1063/1.5053132 PMID: 31042969

64. Wu X, Zi F, Dudley J, Bilotta RJ, Canoza P, Müller H. Multiaxis atom interferometry with a single-diode laser and a pyramidal magneto-optical trap. Optica. 2017; 4(12):1545–1551. https://doi.org/10.1364/OPTICA.4.001545

65. Kovachy T, Asenbaum P, Overstreet C, Donnelly C, Dickerson S, Sugarbaker A, et al. Quantum superposition at the half-metre scale. Nature. 2015; 528(7583):530–533. https://doi.org/10.1038/nature16155 PMID: 26701053

66. Salvi L, Poli N, Vuletić V, Tino GM. Squeezing on Momentum States for Atom Interferometry. Phys Rev Lett. 2018; 120:033601. https://doi.org/10.1103/PhysRevLett.120.033601 PMID: 29400516

67. Sugarbaker A, Dickerson SM, Hogan JM, Johnson DMS, Kasevich MA. Enhanced Atom Interferometer Readout through the Application of Phase Shear. Phys Rev Lett. 2013; 111:113002. https://doi.org/10.1103/PhysRevLett.111.113002 PMID: 24074082

68. Yankelev D, Avinadav C, Davidson N, Firstenberg O. Atom interferometry with thousand-fold increase in dynamic range. Science Advances. 2020; 6(45):eabd0650. https://doi.org/10.1126/sciadv.abd0650 PMID: 33148652

69. Berg P, Abend S, Tackmann G, Schubert C, Giese E, Schleich WP, et al. Composite-Light-Pulse Technique for High-Precision Atom Interferometry. Phys Rev Lett. 2015; 114:063002. https://doi.org/10.1103/PhysRevLett.114.063002 PMID: 25723216

70. Mielec N, Altorio M, Sapam R, Horville D, Holleville D, Sidorenkov LA, et al. Atom interferometry with top-hat laser beams. Applied Physics Letters. 2018; 113(16):161108. https://doi.org/10.1063/1.5051663

71. Hobson PJ, Vovrosh J, Stray B, Packer M, Winch J, Holmes N, et al. Bespoke magnetic feld design for a magnetically shielded cold atom interferometer. Sci Rep. 2022; 12:10520. https://doi.org/10.1038/s41598-022-13979-4 PMID: 35732872

72. Shang H, Pan D, Zhang X, Xue X, Shi T, Chen J. Ultrastable laser referenced on velocity-grating atom interferometry. Phys Rev A. 2022; 105:L051101. https://doi.org/10.1103/PhysRevA.105.L051101